

Pactolus I-domain: Functional switching of the Rossmann fold

Mehmet Sen* and Glen B. Legge†

Department of Biology and Biochemistry, University of Houston, 4800 Calhoun, Houston, Texas 77204-5001

ABSTRACT

Murine Pactolus is a neutrophil-specific single chain glycoprotein that plays a role as an apoptosis marker for macrophages. The extracellular region of the protein shows strong sequence similarities to integrin β -subunits. Critical sequence modifications differentiate its function when compared to the integrin family. We show experimentally that Pactolus I-domain does not bind divalent metal ions, indicating that ligand binding is not mediated through a metal ion-dependent adhesion site (MIDAS). NMR data was used to map secondary structure and the strand pairing within the β -sheet to confirm an overall Rossmann fold topology. Homology modeling enhanced by the NMR data was used to determine the overall structure, with two key loop insertions/deletions (insertion 2 and SDL) that distinguish the Pactolus I-domain from the integrin α I-domain and β I-domains. NMR peak exchange broadening is observed due to dimerization, correlating to the β I-domain and β propeller heterodimerization region within the integrin headpiece. Two unique N-linked glycosylation sites (Asn151 and Asn230) within this region disrupt dimerization and may account for why Pactolus is not found to associate with an α -subunit. These changes in quaternary structure, ligand binding loops, glycosylation, and metal sites illustrate how evolution has rapidly and effectively altered key aspects of the integrin β -subunit to derive a protein of novel function on an existing protein scaffold.

Proteins 2007; 68:626–635.
© 2007 Wiley-Liss, Inc.

Key words: *integrin; evolution; metal-binding; function switch; glycosylation; NMR.*

INTRODUCTION

Pactolus was first characterized from mice as a glycoprotein expressed in developing bone marrow cells and stored in cytoplasmic granules that are translocated to the cell surface after neutrophil activation.^{1,2} Pactolus gene is expressed solely in bone marrow cells. Anti-Pactolus antibody screening and gene transcript level of Pactolus shows that maturing and mature neutrophils are the only cells that express Pactolus.¹ The 98 kDa form is expressed and presented on the cell surface, while the 130 kDa form of the Pactolus remains in secretory vesicles in the cytoplasm after expression.³ Activation of the neutrophil by the immune response leads to the shuttling of this form to the cell surface, either as a necrosis signal for macrophages or to interact with another neutrophil.⁴ Pactolus expression helps retain CXCL13-expressing cells at the site of inflammation, with CXCL13 cytokine expression being enhanced by Pactolus expression. However, Pactolus-deficient neutrophils are not preferentially attacked by CXCL13 expressing macrophages.⁴

The Pactolus gene is found on mouse chromosome 16 and shares transcriptional control with its evolutionary paralogues, the β 2- and β 7-integrin subunits⁵ that are located on chromosome 10. Three variants of Pactolus proteins are generated either with or without a transmembrane region and a cytoplasmic tail by alternative splicing mechanisms.⁶ Pactolus is heavily N-linked glycosylated, increasing the apparent molecular weight of the full length protein from 81 kDa to either 98 or 130 kDa.³

This evolutionary similarity to the integrin β -subunits is particularly apparent in the I-domain in the N-terminal region, with a 60% sequence homology to the integrin β 2- and β 7-subunits. However, unlike the integrins, it is not found to associate with an α -subunit.^{1,6} There are also key changes in the sequence of the Pactolus I-domain for each of the three identified integrin β I-domain metal binding sites. The most significant is the presence of a D/G variation for the first residue of the metal ion-dependent adhesion site (MIDAS) DXSXS motif, which is likely to affect divalent metal binding.^{7,8} The MIDAS mediates the direct coordination of the integrin I-domain to a carboxyl group in its target ligand. Moreover, residues are not conserved for the ADjacent to MIDAS (ADMIDAS) (a

The Supplementary Material referred to in this article can be found at <http://www.interscience.wiley.com/jpages/0887-3585/suppmat/>

Grant sponsor: The Welch Foundation; Grant number: E-1580; Grant sponsor: American Heart Foundation Grant; Grant number: 0435123N; Grant sponsor: UH GEAR Grant.

*Current address: Harvard Medical School, CBR Institute for Biomedical Research, 200 Longwood Avenue, Springer Lab, Boston, MA 02115.

†Correspondence to: Glen B. Legge, Department of Biochemistry, University of Houston, 4800 Calhoun, Houston, TX 77204-5001. E-mail: glegge@uh.edu

Received 20 September 2006; Revised 18 January 2007; Accepted 22 January 2007

Published online 21 May 2007 in Wiley InterScience (www.interscience.wiley.com). DOI: 10.1002/prot.21458

DD/GH variant) and LIMBS metal sites (a D/N variant).^{9,10} A search of Genbank indicates that a predicted gene (XM_577174) present for *Rattus norvegicus* is similar to Pactolus, and that it contains a similarly mutated MIDAS sequence.

Like the integrin α I-domain, the Pactolus I-domain also lacks the specificity determining loop (SDL), which is a significant determinant of ligand-binding specificity for the integrin β -subunit.¹¹ Within the Rossmann fold of the β I-domain, the SDL region consists of an \sim 30-residue disulfide-bridged loop between the β 2 and β 3 strands.^{1,6,12} Recent studies¹³ also conclude that the SDL is responsible for defects in integrin β -subunit expression and folding in the absence of α -subunits. Deletion of the SDL, thus mimicking Pactolus, enables autonomous folding of integrin β -subunits.

In this paper, we use NMR experimental data to enhance modeling of the Pactolus I-domain and to investigate how changes in the key determinants of integrin function have affected the Rossmann fold scaffold.

MATERIALS AND METHODS

Expression, refolding, and purification

The recombinant Pactolus I-domain gene used for these studies corresponds to amino acid residues 124–333 of the Pactolus gene (Genebank Accession #AF051367). This domain was kindly supplied by Prof. Yoshikazu Takada (UC-Davis) and was inserted into pET28a with an N-terminal 6His affinity tag. Recombinant Pactolus I-domain was transformed in *Escherichia coli* BL21(DE3) RP cells (Stratagene, Inc.), and the cells were grown at 37°C. The samples were prepared in minimal medium containing M9 salts, supplemented with 1 \times BME Vitamins solution (Sigma-Aldrich), 4 g/L D-glucose and induced with IPTG (1 mM) when OD_{600 nm} = 0.6 and incubated at 37°C overnight. For isotopically labeled samples, ¹⁵NH₄Cl, (¹⁵NH₄)₂SO₄, and [¹³C₆]D-glucose (Isotech Laboratories) were used as the sole nitrogen and carbon sources. For the triple-labeled sample, 99.7% ²H₂O replaced standard milli-Q ¹H₂O. Up to 80 mg/L protein by SDS PAGE expressed as inclusion bodies.

A harvested cell pellet from 1 L of culture was resuspended in 1 \times PBS and lysed by sonication, and the homogenate was centrifuged. The resulting supernatant was discarded and the pellet was resuspended and washed an additional three times. The washed pellet was solubilized overnight at 4°C in 6M urea, 20 mM Tris (pH 8.0), and centrifuged at \sim 10,000g for 30 min, then filtered (0.45 μ m) and loaded onto a Ni-NTA column (GE Healthcare). Bound protein then was eluted with solubilization buffer and 250 mM imidazole prior to overnight dialysis at 4°C against refolding buffer [20 mM Tris (pH 8.0) and 300 mM NaCl]. The recovered dialyzate was centrifuged to remove any precipitate present, concentrated to 2 mL

Table 1
Hydrogen Bond Donors and Predicted Acceptors

	Donor		Predicted acceptor			ss
106	ASP	HN	202	ARG	0	β 1
107	LEU	HN	143	ARG	0	β 1
109	PHE	HN	145	GLY	0	β 1
110	LEU	HN	210	VAL	0	β 1
111	MET	HN	147	GLY	0	β 1
112	GLY	HN	212	VAL	0	β 1
114	SER	HN	117	ALA	0	—
132	LEU	HN	128	GLY	0	α 1
133	LYS	HN	129	SER	0	α 1
134	ALA	HN	130	ASP	0	α 1
135	LEU	HN	131	LEU	0	α 1
143	ARG	HN	105	VAL	0	β 2
144	ILE	HN	161	THR	0	β 2
145	GLY	HN	107	LEU	0	β 2
146	PHE	HN	157	ILE	0	β 2
147	GLY	HN	109	PHE	0	β 2
148	SER	HN	155	GLN	0	β 2
155	GLN	HN	148	SER	0	β 2'
157	ILE	HN	146	PHE	0	β 2'
158	LEU	HN	146	PHE	0	β 2'
170	GLU	HN	166	GLN	0	α 2
171	LEU	HN	167	PHE	0	α 2
196	CYS	HN	192	GLN	0	α 3
202	TRP	HN	197	LEU	0	—
202	TRP	H ϵ 1	192	VAL	0	sc
208	PHE	HN	106	ASP	0	β 3
209	LEU	HN	267	GLN	0	β 3
210	VAL	HN	108	TYR	0	β 3
211	LEU	HN	269	ILE	0	β 3
212	VAL	HN	110	LEU	0	β 3
213	THR	HN	271	VAL	0	β 3
267	GLN	HN	207	ARG	0	β 4
269	ILE	HN	209	LEU	0	β 4
270	PHE	HN	291	THR	0	β 4
271	VAL	HN	211	LEU	0	β 4
272	VAL	HN	293	GLY	0	β 4
291	THR	HN	268	PRO	0	β 5
293	GLY	HN	270	PHE	0	β 5
295	LEU	HN	272	VAL	0	β 5
305	LEU	HN	303	ALA	0	α 6
306	ILE	HN	302	VAL	0	α 6

Hydrogen bond restraints were only included in the structure calculations if the amide proton showed strong H/D exchange protection, and that a hydrogen bond acceptor could be unambiguously defined. The region of secondary structure where the hydrogen bond is found is indicated in the ss column; with a potential hydrogen bond acceptor for the insertion 2 residue Thr246 (in2) and the Trp 224 H ϵ 1 also uniquely identified (sc). Assigned H/D protected residues outside of regular secondary structure are shown as a dash.

using Centriprep 10K (Millipore), and loaded onto a Superdex 75 Size Exclusion column (GE Healthcare) with a mobile phase of 20 mM Tris (pH 8.0), 100 mM NaCl. The Pactolus I-domain fractions corresponding to the monomer were pooled and concentrated using a Centricon (Millipore) device. For NMR data acquisition, a 0.5 mM sample of purified and uniformly isotopically labeled Pactolus I-domain was prepared in 10 mM dTris (pH 6.8), 0.05% (w/v) NaN₃, and 5% ²H₂O, with a Shigemi microcell employed for each sample.

NMR titration with Mg²⁺, Ca²⁺

Chelex deionized buffers were prepared largely as described,¹⁴ with all labware used for these procedures (and in subsequent handling of samples) pretreated with EDTA. Samples were prepared in ion-free water containing 20 mM dTris (pH 6.9) for both NMR titrations and ITC. A 250 μ M ¹³C/¹⁵N-labeled cation-free sample of the Pactolus I-domain was titrated with 5 mM CaCl₂. For the Mg²⁺ titrations, a 200 μ M ¹H/¹⁵N-labeled sample of cation-free Pactolus I-domain was titrated with 5 mM MgCl₂. For all titrations, changes were observed by acquisition of the ¹H/¹⁵N HSQC spectra on a DRX 600 MHz Bruker spectrometer at 298 K by four scans per increment.

Gel filtration chromatography

Size exclusion chromatography of the ¹⁵N-labeled Pactolus I-domain NMR sample was performed using in the Sephadex-75 Size exclusion column with a mobile phase of 20 mM Tris (pH 8.0), 100 mM NaCl at 4°C, at a flow rate of 1 mL/min. Phenomenex size exclusion molecular weight standards (Cat. #ALO3042) were used to calibrate the size exclusion retention time versus logarithm of molecular weight. Molecular weights of the ¹⁵N-labeled Pactolus I-domain NMR sample were calculated using retention times of the sample OD_{280 nm} peaks based on a previously prepared standard curve.

NMR assignments

Sequential backbone resonance assignments were carried out using isotopically ²H/¹³C/¹⁵N- and ¹³C/¹⁵N-labeled samples of the Pactolus I-domain using through-bond triple resonance methods. These data sets included HNCA,^{15,16} HN(CO)CA,^{15,16} HNCACB,^{17,18} HN(CO)CACB,^{17,18} HNCO,^{15,16} HN(CA)CO,^{15,16} on a Bruker 800 MHz spectrometer at 298 K equipped with a TXI probe. An additional HN(CA)CO data set was acquired using a cryogenic probe courtesy of Bruker Biospin. Data were processed and analyzed using NMRPipe¹⁹ and NMRView.²⁰

Distance and hydrogen/deuterium exchange derived restraints

Interproton distance restraints were obtained from ¹H/¹⁵N HSQC–NOESY–HSQC^{21,22} and CN–NOESY²³ spectra with a 150 ms mixing time. Partial side chain assignments were determined by analysis of the CN–NOESY to give H α , H β , and HN proton resonances. Because of homodimerization of the Pactolus I-domain and the necessity for the sample to be deuterated, few side chain proton assignments could be determined. Assigned NOE peaks were incorporated as either strong (>2.8 Å), medium (>3.5 Å), or weak (>5.0 Å) into the

subsequent structure calculations. Pseudoatom expansion corrections were applied where stereo assignments were not determined.

For the amide exchange experiments, a 0.25 mM sample of ¹³C/¹⁵N-labeled Pactolus I-domain in 10 mM dTris (pH 6.8), 0.05% NaN₃ was prepared and buffer exchanged into 10 mM dTris (pH 6.8), 100% ²H₂O by using NAP-5 column (GE Healthcare). A series of ¹H/¹⁵N HSQC spectra of the ²H₂O sample were acquired after 5 min, 1, 6, and 24 h to identify amide protons that were resistant to deuterium exchange. Hydrogen bond donor protons were paired with likely acceptor partners from NOE and H/D exchange, and these were included in the subsequent structure calculations as distance restraints.

ψ and ϕ restraints based on deviation from random coil chemical shifts

A correlation between backbone ψ and ϕ dihedral angles and the deviation from random coil ¹³C α chemical shift values and the chemical shift index (CSI) has been demonstrated.^{24,25} Each residue's CSI was calculated using a weighted CSI program, written by Kyoko Yap (<http://nmr.uhnres.utoronto.ca/ikura/csi/>), that incorporates both the ¹³C α and ¹³C β shifts for residue (*i*) and neighboring residues (*i*±1) by following equation:

$$CSI = \frac{\delta[C_{\alpha(i-1)} - C_{\beta(i-1)}] + 2\delta[C_{\alpha(i)} - C_{\beta(i)}] + \delta[C_{\alpha(i+1)} - C_{\beta(i+1)}]}{4}$$

where δC_{β} and δC_{α} are the ¹³C chemical shifts minus the average ¹³C α or ¹³C β random coil chemical shifts for that residue type. Dihedral angle restraints were used during structure calculations for residues that could be defined as belonging to either α or β secondary structure from the CSI data. These restraints were applied as $-150 \leq \phi \leq -20$, $-80 \leq \psi \leq 20$ for α -helical regions; and as $-180 \leq \phi \leq -40$, $50 \leq \psi \leq -150$ for β -sheet regions.

Calculation of NMR-enhanced models

Using the torsion angle dynamics program DYANA,²⁶ 200 structures were calculated with the experimentally derived restraints, with the 100 lowest energy further refined by homology modeling with Modeller8v2,²⁷ where the β 3 I-domain (residues Pro111 to Ser353) from the α V β 3 crystal structure (pdb#1JV2) was used as a template. This was necessary for regions where NMR exchange broadening gave little NMR data. The result of these calculations were then verified against the NMR experimental data by minimization in the Sander module of AMBER8.²⁸ All AMBER calculations were performed on SGI clusters (IMD UH). PROCHECK_NMR²⁹ was used to analyze the quality of the refined structures.

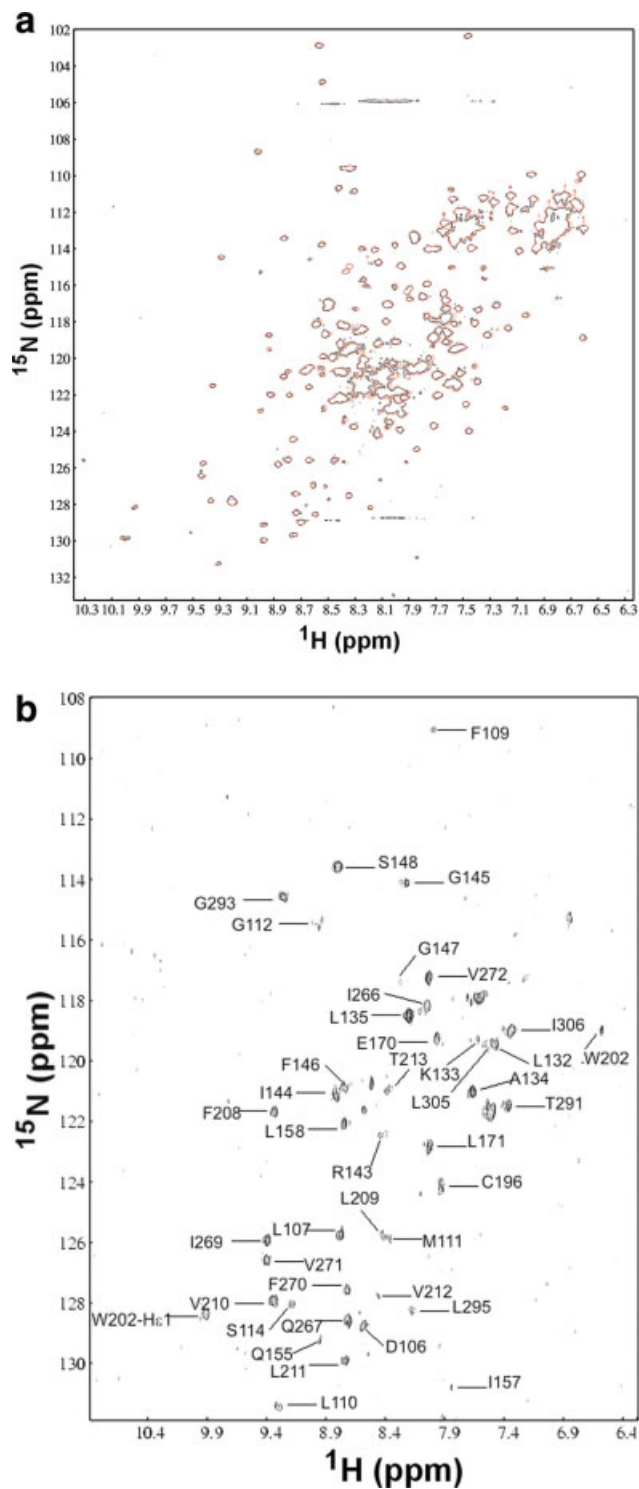


Figure 1

a) $^1\text{H}/^{15}\text{N}$ HSQC spectrum of a 250 μM Pactolus I-domain sample with either 0 or 5 mM Mg^{2+} (shown as black and red respectively) in 20 mM dTris-HCl at pH 6.9, 4 scans acquired on a 600 MHz Bruker Spectrometer. **b)** A $^1\text{H}/^{15}\text{N}$ HSQC spectrum of Pactolus I-domain in 99.7% $^2\text{H}_2\text{O}$, $\text{pD}^+ = 6.3$, with the peaks that are resistant to amide proton exchange following 5 hours at 298 K are shown by their sequence specific assignment.

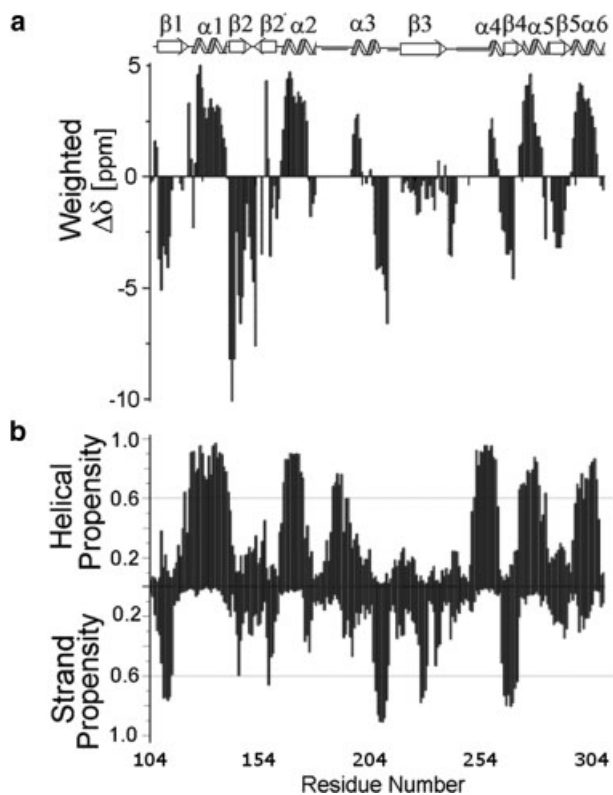


Figure 2

a) Weighted Chemical Shift Index showing the secondary structure elements of the Pactolus I-domain. Boundaries of the helices and strands are shown above the figure, with regions that have missing assignments highlighted in red. **b)** Secondary structure analysis based on primary sequence of Pactolus I-domain as calculated by JUFO, where highest propensity is 1, and the lowest propensity is 0. A line shown at the 0.6 to indicate regions that show either strong helical (upward) or strand (downward) propensity.

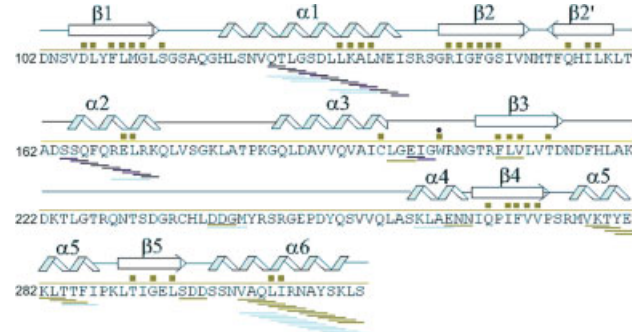


Figure 3

The Pactolus I-domain primary sequence indicating the location of the exchange-protected amides after 5 hours at 298 K (green squares). The elements of secondary structure based on CSI are also shown, together with the HN-HN NOEs from NOESY spectra that are indicative of helix. The $d_{\text{NN}}(i,i+1)$ NOEs are shown in purple, $d_{\text{NN}}(i,i+2)$ NOEs are shown green and $d_{\text{NN}}(i,i+3)$ NOEs are shown in blue.

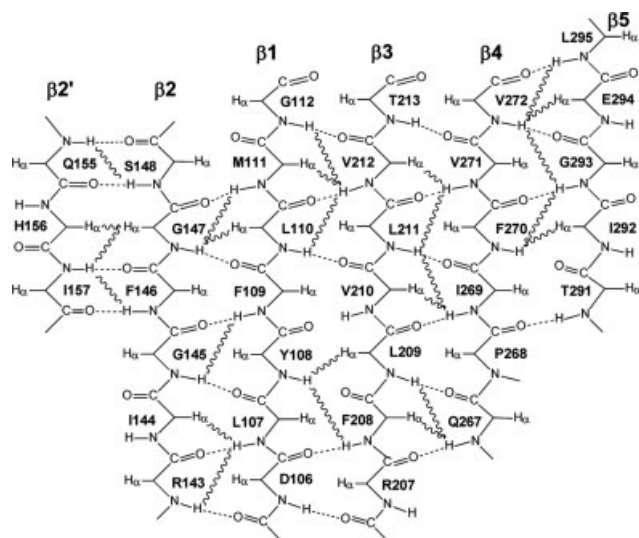


Figure 4

Parallel and antiparallel β -structure in the Pactolus I-domain, with observed NOEs indicated by a wavy line, and the predicted hydrogen bonds from solvent exchange protected amides is shown as a dashed line. Figure was generated using ChemDraw Ultra10.0 (CambridgeSoft Corporation).

RESULTS

NMR sequence-specific assignments

A primary peak count of the $^1\text{H}/^{15}\text{N}$ HSQC spectra of the Pactolus I-domain revealed 182 readily resolvable peaks from a 0.4 mM $^2\text{H}/^{13}\text{C}/^{15}\text{N}$ -labeled sample, if the side chain $-\text{NH}_2$ resonances were ignored. Most assignments were subsequently obtained from this sample by analysis of triple resonance heteronuclear NMR spectra to give 84% for $\text{C}\alpha$, 81% for $\text{C}\beta$, 84% for CO , and 84% for ^{15}N , and 85% for ^{13}C backbone resonances [Fig. 1(a)]. Additional $^1\text{H}\alpha$ resonances were obtained from analysis of the heteronuclear NOESY spectra from a $^1\text{H}/^{15}\text{N}$ -labeled sample.

Pactolus I-domain does not bind divalent cations

To experimentally identify if the Pactolus I-domain binds an Mg^{2+} cation for its function, we prepared a $^1\text{H}/^{15}\text{N}$ - or a $^1\text{H}/^{13}\text{C}/^{15}\text{N}$ -labeled recombinant Pactolus I-domain in deionized chelex water as described.¹⁴ Evidence of the Pactolus I-domain binding of divalent cations was monitored by $^1\text{H}/^{15}\text{N}$ HSQC spectra of the Pactolus I-domain acquired upon titrating increasing amount of Mg^{2+} [Fig. 1(a)] and Ca^{2+} (data not shown). Titration using Mg^{2+} followed by back titration with EDTA showed no evidence of a significant interaction of the divalent metal with the protein in the NMR spectra.

Dimerization of the pactolus I-domain

Residues to which resonance assignments could not be sequentially assigned clustered to three regions in the sequence (Leu180–Ile195, Asn215–Ala220, and Ser245–Leu261). To investigate whether this is due to dimerization, a 0.4 mM ^{15}N -labeled Pactolus I-domain NMR sample was injected into a Superdex 75 size exclusion column (GE Healthcare), which generated two peaks (supplementary data). Using molecular weight standards, the secondary peak was calculated to be approximately 52 kDa, which corresponds to a homodimeric Pactolus I-domain. Dimerization of the domain would also account for the poor NMR relaxation characteristics of the protein in solution and the intermediate exchange broadening at the dimer interface.

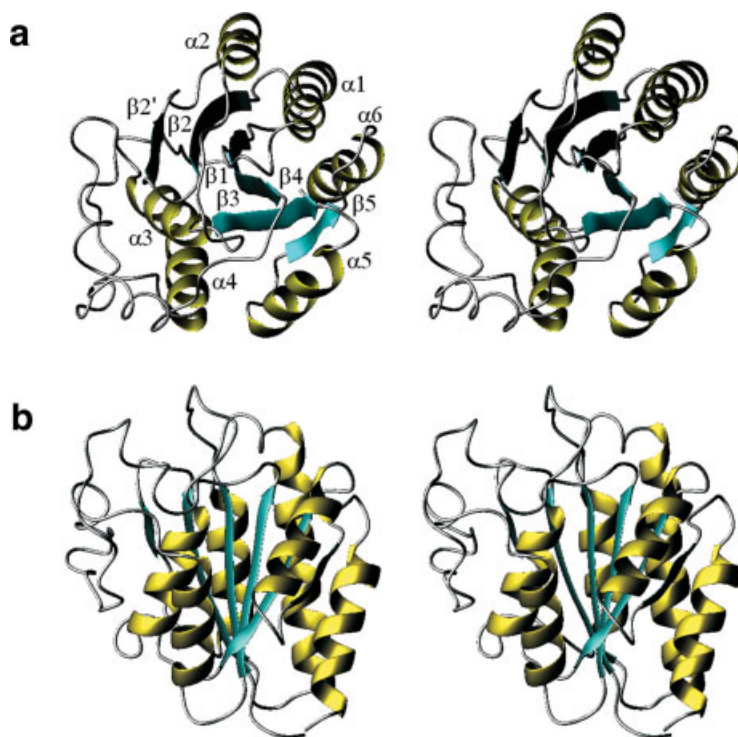
NMR restraints

NOEs that are characteristic of either α -helix or β -strands correlate well with the predicted CSI secondary structure boundaries. NOE-based distance restraints used in the structure calculation were derived from heteronuclear isotope edited $^{13}\text{C}/^{15}\text{N}$ NOESY spectra. NOE cross-

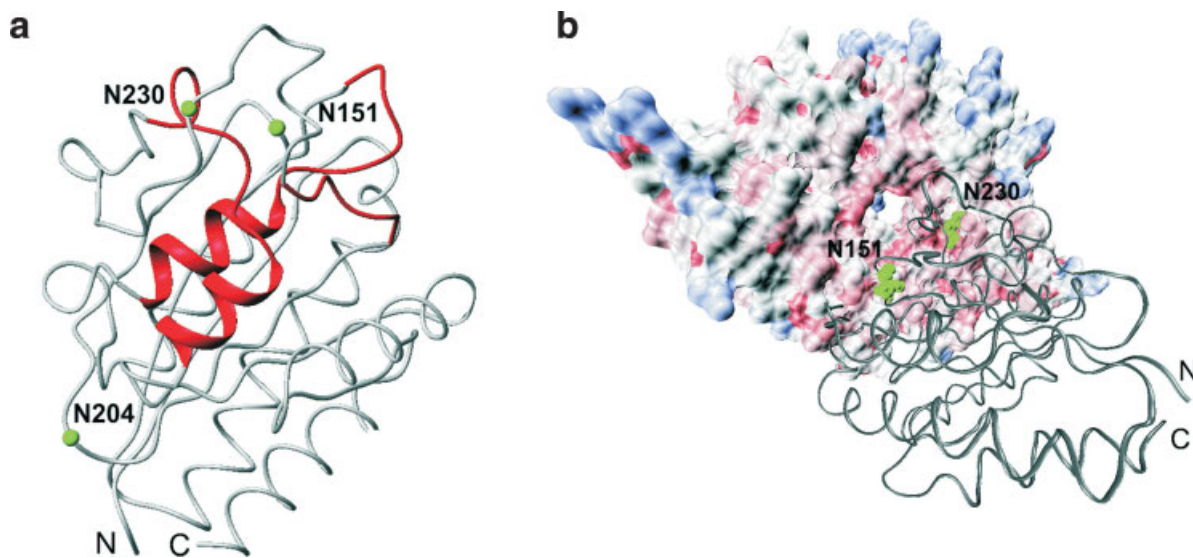
Table II

Summary of the Number of Restraints Used in the Calculations and Structural Statistics for the 20 Final NMR-Enhanced Models

Restraint Classification	
Total NOE	195
Sequential ($ i - j = 1$)	87
Medium-range ($ i - j \leq 4$)	69
Long-range ($ i - j \geq 5$)	38
Hydrogen-bond restraints	47
Total dihedral angle restraints	180
ϕ (CSI)	90
ψ (CSI)	90
Amber minimization RMSD following Modeller8v2	
Mean RMSD change (backbone) (\AA)	0.4
Maximum RMSD change (backbone) (\AA)	0.4
Mean RMSD change (heavy) (\AA)	0.5
Maximum RMSD change (heavy) (\AA)	0.6
Amber structural statistics	
Maximum distance restraint violation (\AA)	0.42
Mean constraint violation energy (kcal mol^{-1})	86.67
Mean Amber energy (kcal mol^{-1})	-5808.83
Maximum dihedral angle violation ($^\circ$)	4.6
Average pairwise RMSD (\AA)	
Heavy (residues 126–333)	1.36
Backbone (residues 126–333)	0.85
PROCHECK statistics for ϕ and ψ	
Most favored (%)	83.0
Allowed favored (%)	14.6
Generously allowed (%)	2.1
Disallowed (%)	0.3
Template/minimized model RMSD	
Template (pdb#1JV2)/lowest energy model	
Backbone RMSD (\AA) from VMD ³⁴	1.6

**Figure 5**

a) Annotated ribbon diagram of the backbone of the lowest energy NMR enhanced model structures of the Pactolus I-domain. b) Ribbon diagram shown rotated by 90° along the x-axis as compared with a). Both figures are stereo-views of residues Ser126–Lys236, where α -helices are colored yellow, β -strands are blue, and loops/turns are grey. Figures were generated using the program MOLMOL.⁴⁰

**Figure 6**

Pactolus I-domain forms a dimer in the solution a) Ribbon diagram of the lowest energy structure with the three unassigned regions (Leu180–Ile195, Asn215–Ala220, and Ser245–Leu261) highlighted and labeled in red and the predicted N-glycosylation sites in green as depicted with the program MOLMOL.⁴⁰ b) The two potential N-linked glycosylation residues of Pactolus I-domain (Asn151 and Asn230) may disrupt the formation of an integrin headpiece. The β -propeller domain within the $\alpha\beta 3$ crystal structure (pdb#1JV2) is shown as an electrostatic surface plot, the Pactolus I-domain (superimposed and replacing the $\beta 3$ I-domain within the $\alpha\beta 3$ crystal structure) is shown as a backbone tube and potential glycosylation sites in the interface are shown in green as CPK using VMD.³⁴

peaks were assigned de novo and then cross-checked against the $\beta 3$ I-domain X-ray structure and αL I-domain solution structure.^{9,30} The $d_{NN}(i,j)$ cross-strand and the medium range $d_{NN}(i,i+3)$ and $d_{\alpha N}(i,i+4)$ NOEs were used to define regions of secondary structure and are illustrated in Figure 3(b,c). The peptide bonds for all proline residues were identified as “trans” based on $^{13}\text{C}\alpha$ and $^{13}\text{C}\beta$ chemical shifts.

Amide proton/deuterium exchange protection correlates to the hydrogen bonding pattern within a protein.³¹ For the Pactolus I-domain, there were 47 cross-peaks that exchange protected [Fig. 1(b)], and 35 present overnight. This indicates the presence of a stable protein core, and likely hydrogen bond acceptor partners were identified using the NMR data (Table I). Identified residues that show deuterium exchange protection are consistent with the secondary structure hydrogen bonding pattern, with only the $\alpha 4$ and the C-terminal $\alpha 6$ helices showing decreased protection.

Best fit analysis of Pactolus I-domain circular dichroism (CD) spectra to a linear combination of standard dichroic spectra for secondary structure elements³² was used to estimate a structural composition of 37% α -helix and 14% β -sheet (supplementary data). Analysis of the $\text{C}\alpha$, and to a lesser extent the $\text{C}\beta$, chemical shift index (CSI) identified six β -strands and six regions of α -helical structure [Fig. 2(a)]. Only a limited subset of NOEs could be identified due to homodimerization of the Pactolus I-domain. Even so, the NMR data extended the identified regions of secondary structure to uniquely identifying the cross-strand β -sheet pairing and the $i-i+4$ hydrogen bonding interactions within the helices (Figs. 3 and 4).

NMR-enhanced model

NMR data was used to experimentally refine the structures generated from modeling with the integrin $\beta 3$ I-domain from the crystal structure of $\alpha V\beta 3$ as a template (pdb#1JV2). Structures were obtained using a protocol of initial calculations using DYANA,²⁶ modeling using Modeller8v2, and minimization with the NMR restraints reapplied using AMBER8.²⁸ An AMBER minimization with the NMR restraints reapplied, resulted in only small deviations from the modeled structures (Table II). The 20 structures with the lowest torsion angle energies, restraint violation energies and AMBER energies were selected for analysis, as summarized in Table II and shown in Figure 5(a). The models show excellent agreement with the experimental NMR data, with no violations of distance restraints greater than 0.4 Å, and no angle violations greater than 4.6° (Table II). The root mean square deviation (RMSD) for backbone heavy-atoms from residues 126–336 for the 20 AMBER minimized NMR-enhanced models was 0.8 Å.

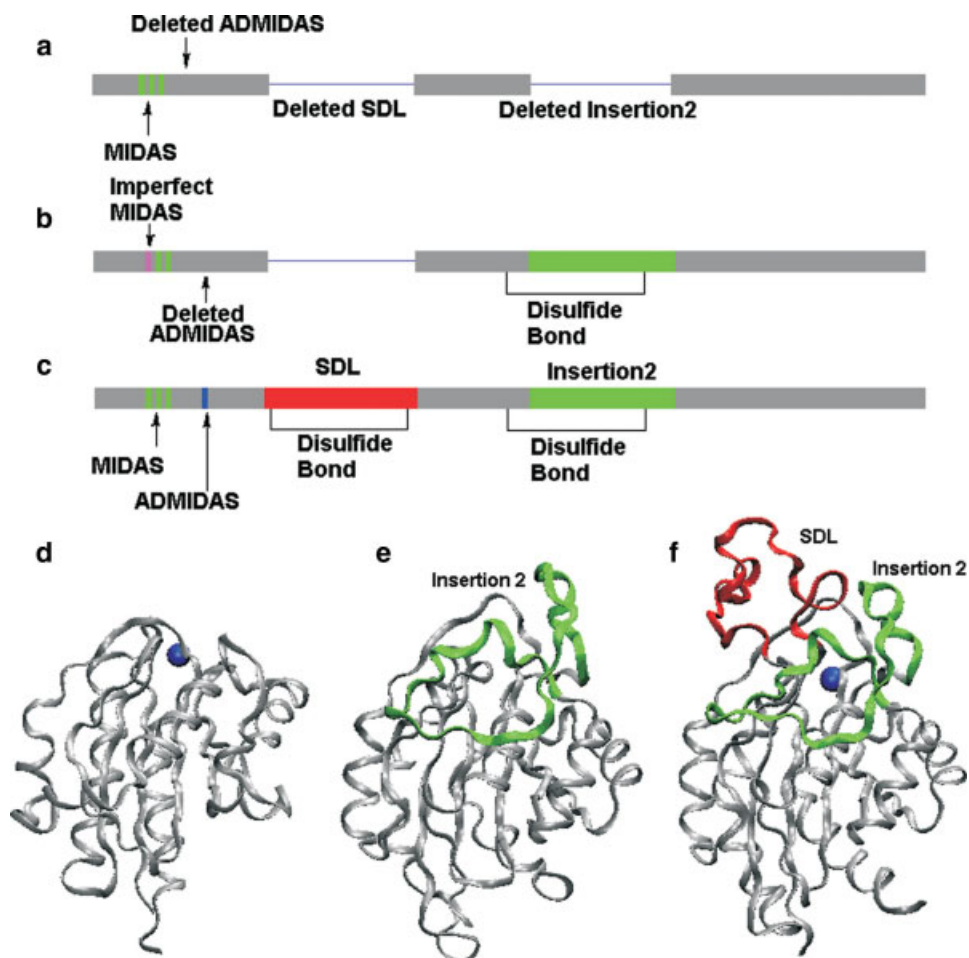
Within the calculated structures, the boundaries of the regions of secondary structure were identified using the

program PROMOTIF³³ and show good correlation to the CSI [Fig. 5(b)]. The models also agree well with the cross-strand β -sheet pairing and helical hydrogen bond formation shown in Figure 3. The overall topology of the Pactolus I-domain structure is that of a Rossmann fold, which consists of a central parallel β -sheet composed of five strands and an additional short antiparallel β -sheet, surrounded by seven amphipathic α -helices [Fig. 5(b)]. The topology is similar to that of its integrin $\beta 3$ I-domain template structure (pdb#1JV2), with the backbone RMSD between the template and the lowest energy model I-domain is 1.6 Å using the stamp module in VMD.³⁴ However, in the Pactolus structure the SDL is replaced by a short turn formed between residues V172–F176.

DISCUSSION

The most significant change which differentiates the function of Pactolus from the integrins is the Asp to Gly modification at the MIDAS. NMR and ITC titrations demonstrate that the Pactolus I-domain does not interact with magnesium cations, indicating that, unlike the integrin I-domains, it cannot mediate a metal ion-dependant carboxyl ligand interaction. The Asp–Asp motif of ADMIDAS and the Asp of LIMBS are also mutated to Gly–His and Asn respectively, further contributing to a loss of metal divalent cation occupancy of the Pactolus I-domain. Coordination of a carboxyl group to a divalent metal at the MIDAS is the hallmark of integrin–ligand interactions. Therefore, these key mutations preclude Pactolus–ligand binding via the same metal ion-independent mechanism for integrin–ligand interactions. Though the MIDAS region within Pactolus I-domain may still remain the primary point of interaction with an as yet unidentified and ligand. Alternatively, Pactolus may interact with other proteins or ligands primarily through its saccharide coat.

Two insertions, the SDL and insertion 2, structurally distinguish the integrin β I-domain to the α I-domain. The Pactolus I-domain has only one of these two insertions (insertion 2, Leu219–Pro259) located between the $\beta 3$ -strand and the $\alpha 4$ helix^{9,35,36} (Figs. 6 and 7). In integrins, the insertion 2 region is hydrophobic and essential for the formation of the integrin-headpiece through its dimerization with the β -propeller domain within the α -subunit. Replacing a short region within the integrin $\beta 3$ -subunit (GIVQP), with the more hydrophilic residues found in Pactolus (TRQNT) prevented the association with an $\alpha 5$ -subunit.^{13,30} The Pactolus I-domain is structurally similar to the α -subunit I-domain^{9,35,36} in that they each lack an SDL, with the loop between $\beta 2$ and $\beta 3$ sheets four (pactolus) or three (integrins) residues long and linked by a tight turn (Figs. 6 and 7). In integrins, this SDL region is critical for the specificity of

**Figure 7**

Annotated cartoon of the primary sequence illustrating metal binding sites and insertions/deletions from the **a**) integrin α -subunit I-domain **b**) Pactolus I-domain and **c**) integrin β -subunit I-domain. Ribbon diagram depicting the structural differences between the: **d**) LEA1 α -subunit I-domain (pdb#1lfa1); **e**) NMR enhanced model of the Pactolus I-domain; and **f**) β 3 I-domain (right) (pdb# 1JV2). The SDL is shown in red and Insertion 2 is shown in green, and with divalent cations depicted as a blue CPK sphere using VMD.³⁴

the β I-domain for its ligand,¹¹ but is not critical for the formation of the $\alpha\beta$ heterodimer.^{13,30}

N-linked glycosylation is the major posttranslational modification identified in Pactolus.³ Moreover, changing the N-glycan structures³⁷ or introducing de novo glycosylation sites³⁸ within an integrin β -subunit is known to alter its function. Two of three potential N-linked (Asn–X–Ser/Thr) glycosylation sites, Asn151 (in the turn between β 2 and β 2') and Asn230 (in the center of insertion 2), are unique to Pactolus and a third site (Asn204) is common among integrin β -subunits.¹³ Within Pactolus, the unique glycosylation sites are near the recombinant protein homodimerization site [Fig. 6(a)]. These N-linked glycosylation sites, when superimposed onto the β 3 I-domain in α V β 3 (pdb#1JV2), lie at the interface of the β I-domain and the β -propeller which form the

integrin headpiece^{10,30} [Fig. 6(b)]. Thus, glycosylation of the native protein may prevent homodimerization or heterodimerization with an α -subunit.

Within the literature, it is generally accepted that two proteins with more than 25% sequence homology will correlate not only their structure, but also their function³⁹. However, Pactolus is a fascinating example in which the overall structural and sequence conservation is not correlated with a conservation of function. With a 60% sequence homology to the integrins, Pactolus clearly shows that there may not always be a direct correlation of sequence conservation and protein function. Indeed, all the changes, including $\alpha\beta$ heterodimerization, MIDAS-mediated binding, glycosylation, and interaction of the SDL with its ligand, affect the essential determinants of integrin function. Thus in the divergence and evolution of

Pactolus, our model indicates the changes that have occurred resulted in the alteration of key aspects of integrin function, while maintaining an overall protein scaffold.

Supplementary materials

The backbone ^1H , ^{15}N , and ^{13}C chemical shifts for the Pactolus I-domain have been deposited to the BioMagResBank (<http://www.bmrb.wisc.edu>) under accession number 7313. Coordinates for the 20 structures of the Pactolus I-domain with the lowest AMBER energy, and NMR restraints are deposited in the RCSB Protein Data Bank www.pdb.org under the accession number 2IUE. CD spectra and a size exclusion chromatography trace are provided as supplementary data.

ACKNOWLEDGMENTS

We thank Professor Yoshikazu Takada for providing the Pactolus I-domain clone, Drs. Youlin Xia (UH Keck IMD NMR Center) and Helena Kovacs (Bruker Biospin) for NMR data acquisition, and Tatsuo Yamakawa, Andrea L. Creath and John J. Craft, Jr. for help in the preparation of this manuscript.

REFERENCES

- Chen Y, Garrison S, Weis JJ, Weis JH. Identification of pactolus, an integrin beta subunit-like cell-surface protein preferentially expressed by cells of the bone marrow. *J Biol Chem* 1998;273:8711–8718.
- Garrison S, Hojgaard A, Margraf R, Weis JJ, Weis JH. Surface translocation of pactolus is induced by cell activation and death, but is not required for neutrophil migration and function. *J Immunol* 2003;171:6795–6806.
- Garrison S, Hojgaard A, Patillo D, Weis JJ, Weis JH. Functional characterization of Pactolus, a beta-integrin-like protein preferentially expressed by neutrophils. *J Biol Chem* 2001;276:35500–35511.
- Hojgaard A, Close R, Dunn DM, Weiss RB, Weis JJ, Weis JH. Altered localization of CXCL13 expressing cells in mice deficient in Pactolus following an inflammatory stimulus. *Immunology* 2006;119:212–223.
- Hale JS, Dahlem TJ, Margraf RL, Debnath I, Weis JJ, Weis JH. Transcriptional control of Pactolus: evidence of a negative control region and comparison with its evolutionary paralogue, CD18 (beta2 integrin). *J Leukoc Biol* 2006;80:383–398.
- Margraf RL, Chen Y, Garrison S, Weis JJ, Weis JH. Genomic organization, chromosomal localization, and transcriptional variants of the murine Pactolus gene. *Mamm Genome* 1999;10:1075–1081.
- Emsley J, Knight CG, Farnsdale RW, Barnes MJ, Liddington RC. Structural basis of collagen recognition by integrin alpha2beta1. *Cell* 2000;101:47–56.
- Shimaoka M, Takagi J, Springer TA. Conformational regulation of integrin structure and function. *Annu Rev Biophys Biomol Struct* 2002;31:485–516.
- Legge GB, Kriwacki RW, Chung J, Hommel U, Ramage P, Case DA, Dyson HJ, Wright PE. NMR solution structure of the inserted domain of human leukocyte function associated antigen-1. *J Mol Biol* 2000;295:1251–1264.
- Xiong JP, Stehle T, Zhang R, Joachimiak A, Frech M, Goodman SL, Arnaout MA. Crystal structure of the extracellular segment of integrin alpha Vbeta3 in complex with an Arg–Gly–Asp ligand. *Science* 2002;296:151–155.
- Takagi J, Kamata T, Meredith J, Puzon-McLaughlin W, Takada Y. Changing ligand specificities of alphavbeta1 and alphavbeta3 integrins by swapping a short diverse sequence of the beta subunit. *J Biol Chem* 1997;272:19794–19800.
- Tuckwell DS, Humphries MJ. A structure prediction for the ligand-binding region of the integrin beta subunit: evidence for the presence of a von Willebrand factor A domain. *FEBS Lett* 1997;400:297–303.
- Takagi J, DeBottis DP, Erickson HP, Springer TA. The role of the specificity-determining loop of the integrin beta subunit I-like domain in autonomous expression, association with the alpha subunit, and ligand binding. *Biochemistry* 2002;41:4339–4347.
- Veeraraghavan S, Fagan PA, Hu H, Lee V, Harper JF, Huang B, Chazin WJ. Structural independence of the two EF-hand domains of caltractin. *J Biol Chem* 2002;277:28564–28571.
- Kay LE, Xu GY, Yamazaki T. Enhanced-sensitivity triple-resonance spectroscopy with minimal H_2O saturation. *J Magn Reson A* 1994;109:203–216.
- Schleucher J, Sattler M, Grundstrom T. *Angew Chem Int Ed* 1993;32:1489–1491.
- Muhandiram DR, Kay LE. *J Magn Reson B* 2006;103:203–216.
- Wittekind M, Mueller L. HNCACB: a high sensitivity 3D NMR experiment to correlate amide proton and nitrogen resonances with the α -carbon and β -carbon resonances in proteins. *J Magn Reson B* 1993;101:201–205.
- Delaglio F, Grzesiek S, Vuister GW, Zhu G, Pfeifer J, Bax A. NMRPipe: a multidimensional spectral processing system based on UNIX pipes. *J Biomol NMR* 1995;6:277–293.
- Johnson BA. Using NMRView to visualize and analyze the NMR spectra of macromolecules. *Methods Mol Biol* 2004;278:313–352.
- Schleucher J, Schwendinger M, Sattler M, Schmidt P, Schedletsky O, Glaser SJ, Sorensen OW, Griesinger C. *J Biomol NMR* 1994;61:301–306.
- Palmer AG, III, Cavanagh J, Wright PE, Rance M. Sensitivity improvement in proton detected heteronuclear correlation experiments. *J Magn Reson* 1991;93:151–170.
- Xia Y, Yee A, Arrowsmith CH, Gao X. $^1\text{H}(\text{C})$ and $^1\text{H}(\text{N})$ total NOE correlations in a single 3D NMR experiment. ^{15}N and ^{13}C time-sharing in t1 and t2 dimensions for simultaneous data acquisition. *J Biomol NMR* 2003;27:193–203.
- Spera S, Bax A. Empirical correlation between protein backbone conformation and C-alpha and C-beta C-13 nuclear-magnetic-resonance chemical-shifts. *J Am Chem Soc* 1991;113:5490–5492.
- Wishart DS, Sykes BD. The ^{13}C chemical-shift index: a simple method for the identification of protein secondary structure using ^{13}C chemical-shift data. *J Biomol NMR* 1994;4:171–180.
- Guntert P, Mumenthaler C, Wuthrich K. Torsion angle dynamics for NMR structure calculation with the new program DYANA. *J Mol Biol* 1997;273:283–298.
- Fiser A, Do RK, Sali A. Modeling of loops in protein structures. *Protein Sci* 2000;9:1753–1773.
- Case DA, Cheatham TE, III, Darden T, Gohlke H, Luo R, Merz KM, Jr, Onufriev A, Simmerling C, Wang B, Woods RJ. The Amber biomolecular simulation programs. *J Comput Chem* 2005;26:1668–1688.
- Laskowski RA, Rullmann JA, MacArthur MW, Kaptein R, Thornton JM. AQUA and PROCHECK-NMR: programs for checking the quality of protein structures solved by NMR. *J Biomol NMR* 1996;8:477–486.
- Xiong JP, Stehle T, Diefenbach B, Zhang R, Dunker R, Scott DL, Joachimiak A, Goodman SL, Arnaout MA. Crystal structure of the extracellular segment of integrin alpha Vbeta3. *Science* 2001;294:339–345.
- Wuthrich K. *NMR of Proteins and Nucleic Acids*. John Wiley.
- Greenfield N, Fasman GD. Computed circular dichroism spectra for the evaluation of protein conformation. *Biochemistry* 1969;8:4108–4116.
- Hutchinson EG, Thornton JM. PROMOTIF—a program to identify and analyze structural motifs in proteins. *Protein Sci* 1996;5:212–220.

34. Eargle J, Wright D, Luthey-Schulten Z. Multiple alignment of protein structures and sequences for VMD. *Bioinformatics* 2006;22:504–506.
35. Lee JO, Rieu P, Arnaout MA, Liddington R. Crystal structure of the A domain from the alpha subunit of integrin CR3 (CD11b/CD18). *Cell* 1995;80:631–638.
36. Qu A, Leahy DJ. Crystal structure of the I-domain from the CD11a/CD18 (LFA-1, alpha L beta 2) integrin. *Proc Natl Acad Sci USA* 1995;92:10277–10281.
37. Gu J, Taniguchi N. Regulation of integrin functions by N-glycans. *Glycoconj J* 2004;21:9–15.
38. Luo BH, Springer TA, Takagi J. Stabilizing the open conformation of the integrin headpiece with a glycan wedge increases affinity for ligand. *Proc Nat Acad Sci USA* 2003;100:2403–2408.
39. Whittaker CA, Hynes RO. Distribution and evolution of von Willebrand/integrin A domains: widely dispersed domains with roles in cell adhesion and elsewhere. *Mol Biol Cell* 2002;13:3369–3387.
40. Koradi R, Billeter M, Wuthrich K. MOLMOL: a program for display and analysis of macromolecular structures. *J Mol Graph* 1996; 14:51–32.